band gaps of the complete electromagnetic crystal lattice, as denoted by the dots (red online) in Fig. 1. Note that only modes beyond the light line (green online) are capable of propagation. As the band gap of the cladding rings suppresses propagation transverse to the axis, these waveguide modes create efficient energy confinement and propagation along the central core.

The rightmost inset of the figure shows the energy distribution of the fundamental HE_{11} mode within the first electromagnetic band gap, obtained from an effective-index-based eigen-mode simulation using the Lumerical MODE Solutions package [31]. The MPB simulation reveals that approximately 91% of the energy is concentrated within the central channel for this propagating mode, with an intensity profile following approximately Gaussian distribution. A simple mode-matching argument then indicates that efficient excitation of this propagating mode should be achievable with an incident, linearly-polarized Gaussian beam [32].

The waveguide design is scalable in frequency as the normalized axis of the band diagram in Fig. 1 illustrates. In the practical design considered here, a lattice constant of 3 mm is used, resulting in a center core radius of 4.2 mm. The cladding air cylinder radius is slightly reduced to 1.3 mm. The dielectric wall thickness between air cylinders is then 400 μm at its thinnest, providing reasonable mechanical robustness for the initial trial. The dielectric properties of the polymer used in the rapid prototyping process was previously characterized by THz time-domain spectroscopy in our earlier work. From that study, we observed that it has a dielectric constant of 2.75 and loss tangent of 0.02 near 150 GHz [19]. Using these properties, the simulated operating frequency of the fundamental HE_{11} mode is approximately 112 GHz. With these practical design parameters, the intrinsic radiation loss of the HE_{11} mode at 112 GHz (ignoring the material loss) was calculated to be 0.012 dB/mm using Lumerical MODE Solutions.

3.2 Driven mode simulations

In order to estimate the overall propagation loss of the waveguide design including the material loss and effects from other higher-order modes, we then simulated the waveguide under two different excitations, using a finite-difference- time-domain based package (GEMS [33]). The first excitation employed two circular perfect-electric-conductor waveguide feeds inserted into the dielectric waveguide apertures at both ends. Two wave ports excited the TE_{11} mode in the feeds, which then propagated through an 84-mm long electromagnetic crystal waveguide.

Figure 2 depicts the resulting S-parameters. Four passbands are observed around 112, 130, 161 and 182 GHz, corresponding to the band gaps of the original electromagnetic crystal lattice. The field profile in the waveguide at 112 GHz resembles the desired HE_{11} mode as shown in Fig. 1. The 3-dB bandwidth of the first passband centered at 112 GHz is about 15.8 GHz, giving a full bandwidth to mid-gap frequency ratio of 14.1%. The reflection coefficient S_{11} is generally below −30 dB, indicating a very good coupling from the feeding TE_{11} mode to the electromagnetic crystal waveguide modes. Once the S-parameters were obtained, the waveguide power loss factor was calculated by the following equation:

$$\alpha = \ln\left(\frac{|S_{21}|^2}{1-|S_{11}|^2}\right) / (-l), \tag{1}$$

where l is the waveguide length.

#137560- $15.00USD Received 2 Nov 2010; revised 2 Feb 2011; accepted 2 Feb 2011; published 15 Feb 2011

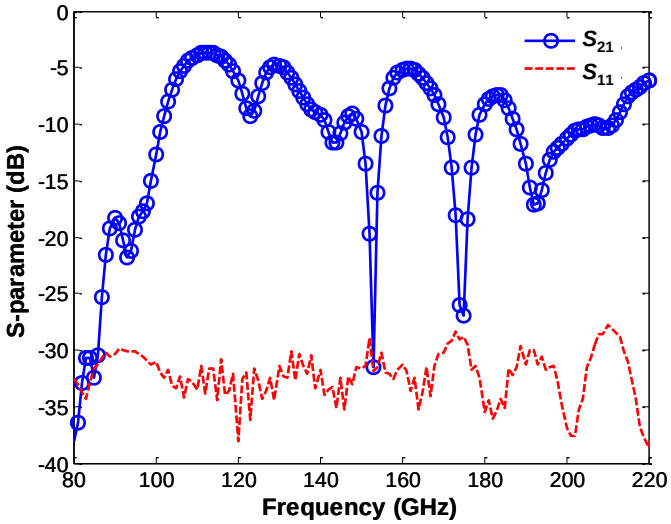

Fig. 2. Simulated S-parameters of an 84 mm-long electromagnetic crystal waveguide.

In a practical experiment, circular metallic waveguide feeds would be inconvenient due to cost and issues in calibrating their losses. Instead, quasi-optical measurement with an incident THz Gaussian beam is preferred. The second simulation is carried out accordingly. In this case, a Gaussian beam of 3-mm beam waist was aimed at the electromagnetic crystal waveguide aperture, and the power flux transmitted out of the other end of the waveguide was calculated. The power flux calculation was performed by integrating the Poynting vector component along the longitudinal direction, S_z, over a surface covering the cross-sectional area of the waveguide. Since the coupling coefficients at the incidence and output ends are identical and independent of the waveguide length, the transmitted power flux has an exponentially decaying relation with waveguide length. A semi-log plot of the transmitted power flux (in dB) versus waveguide length should then be a straight line with a negative slope, which is the intrinsic power loss factor of the waveguide.

This conclusion only holds, however, when multiple reflections within the waveguide are excluded either via time-gating or have negligible magnitudes. Time-domain gating is in principle not quite suitable for electromagnetic crystal waveguide, because it is a highly dispersive system with narrow band features. Its time-domain responses therefore decay very slowly indicating that the multiple reflections mix together, making isolation difficult. However, the assumption that multiple reflections are of negligible magnitude is likely true in our case, as the energy is incident from free space into the air core, and couples to the waveguide propagation modes with an effective refractive index very close to 1 according to Lumerical MODE simulation.

Four waveguides of lengths of 100, 110, 120 and 130 mm were simulated under the same Gaussian beam excitation, and the transmitted power flux in the passbands does indeed show the expected exponential decay as the waveguide length increases. The extracted waveguide loss using these two simulation methods are compared in Fig. 3. The two loss spectra show very good consistency in terms of frequency and depth of the low-loss bands. The lowest propagation loss obtained is 0.022 dB/mm at 112 GHz, which corresponds to a quality (Q) factor of 463 obtained from the formula $Q = \beta/(2\alpha')$, where β is the wave number and $\alpha' = \alpha/2$ is the field attenuation constant, both in linear units. Therefore, the material loss and potential losses from higher-order modes bring in an extra of 0.01 dB/mm loss at this frequency, when compared to the eigen-mode simulation result of the fundamental HE_{11} mode in the last section. Although 5 periods of the cladding lattice was used in the design and practically fabricated later on, simulation proves that 3 periods are adequate to achieve almost identical low-loss propagation.

#137560 - $15.00 USD Received 2 Nov 2010; revised 2 Feb 2011; accepted 2 Feb 2011; published 15 Feb 2011

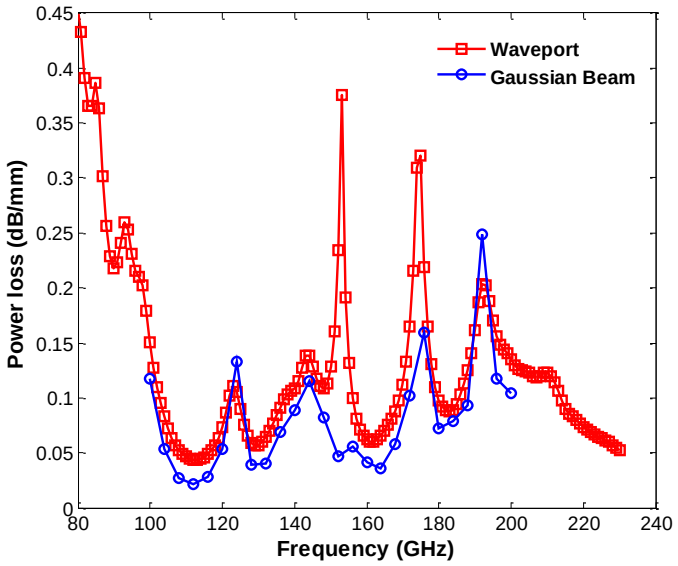

Fig. 3. Power loss factors of the electromagnetic crystal waveguide extracted from the wave port (TE_{11} circular perfect-electric-conductor waveguide feeds) and the Gaussian beam incidence simulations.

4. Experiment

Fabrication of the waveguide was carried out by the aforementioned polymer jetting technique. The structure was printed vertically along the wave channel direction. In this fabrication, the glossy mode with reduced support material usage was applied to minimize surface roughness, as only limited support structure was needed. Figure 4 shows photos of the cross-sectional and full view of a fabricated waveguide.

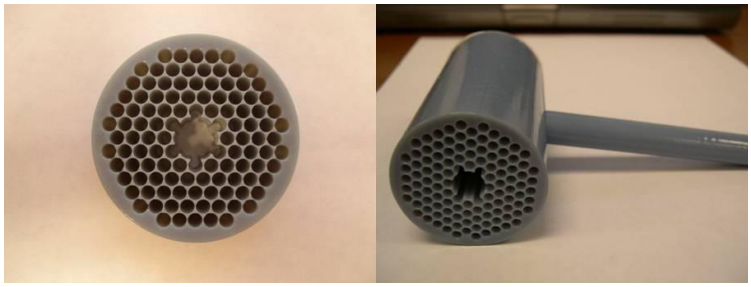

Fig. 4. Cross-sectional and full views of a fabricated THz waveguide, with lattice constant of 3 mm, center core radius of 4.2 mm, and cladding air cylinder radius of 1.3 mm.

A THz time-domain spectroscopy (THz-TDS) system with photoconductive antennas as transmitter and receiver [34] was used for the waveguide characterization. The antennas were able to produce usable spectral content from 50 GHz to 1.2 THz with a peak around 100 GHz. Two off-axis parabolic mirrors with 152.4 mm effective focal length were used to focus the incident beam from the transmitter to a 5.4 mm beam waist. In order to efficiently convert the incident Gaussian beam to the desired HE_{11} waveguide mode, their electric field profiles needed to be well-matched [32]. According to a modal field overlap calculation [32], an optimum beam waist of 2.7 mm would couple the incident Gaussian beam to the waveguide HE_{11} mode with over 90% efficiency. Therefore, a plano-convex polymer lens pair was designed and fabricated by the same rapid prototyping method and used to further focus the beam to the desired size. When placed at the focal point of the off-axis parabolic mirror, the lens focuses the beam to a 2.7 mm waist verified by a razor-blade measurement.

#137560 - $15.00 USD Received 2 Nov 2010; revised 2 Feb 2011; accepted 2 Feb 2011; published 15 Feb 2011

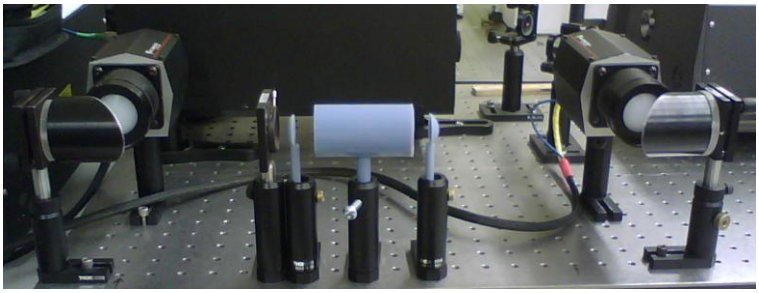

Fig. 5. Setup of the characterization experiment: from left to right: THz transmitter, parabolic mirror 1, iris, polymer lens 1, waveguide under test, polymer lens 2, parabolic mirror 2, and THz receiver. THz time-domain spectrometer used here: T-Ray 2000 turnkey THz system manufactured by Picometrix, Inc.

Figure 5 shows a photo of the quasi-optic setup for waveguide characterization. The iris in the photo was only for the purpose of marking the beam position and opens sufficiently for the entire beam to pass through unobstructed. As discussed previously, waveguides of several lengths needed to be measured in order to characterize the propagation loss factor, similar to the "cut-back" method used in optical fiber loss measurement [35]. Therefore, the spacing between all elements and the waveguide ends were kept the same throughout the measurements to provide an identical optical path with the exception of the waveguide section.

Five waveguides of lengths 50, 75, 100, 125, and 150 mm and identical cross section were placed in the beam path sequentially, and their transmitted waveforms were measured. The two lenses were also positioned 35 mm (17.5 mm x 2) away without a waveguide in between to obtain a reference scan. The spectrometer was set to operate in the long scan mode, covering the entire available time delay range of 1200 pico-second (ps) with a scan speed of 5 ps per second. Each recorded scan was an average of five consecutive scans. The resulted waveforms are shown in Fig. 6(a). The reference scan leads in time, followed by the five waveguide scans with increased delays from the longer waveguides. Dispersion with respect to the reference waveform is observed in all five waveguide scans, which is a clear sign of guided mode resonances. Figure 6(b) plots the power transmittances of all the waveguides, which were obtained by Fourier transforming the waveforms to the frequency domain, then normalizing the spectra with respect to the reference spectrum. Four passbands centered around 105, 123, 153 and 174 GHz can be clearly seen, corresponding to the four passbands in Fig. 2 to within a downshift of a few GHz.

#137560 - $15.00 USD Received 2 Nov 2010; revised 2 Feb 2011; accepted 2 Feb 2011; published 15 Feb 2011

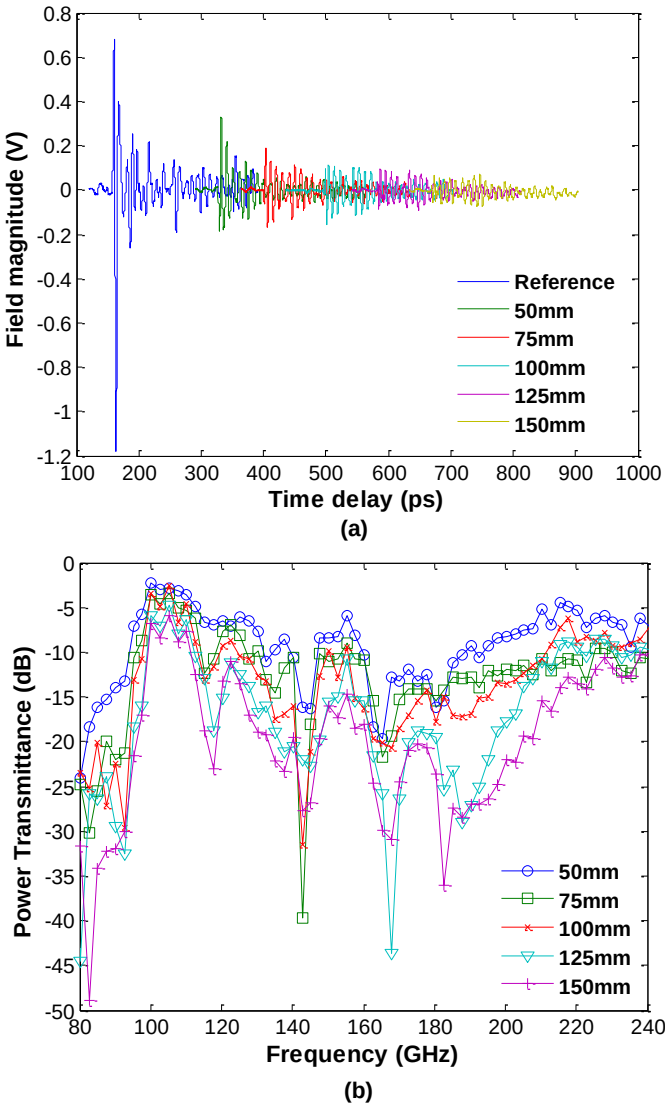

Fig. 6. (a) Transmitted waveforms of five waveguides with different lengths, and the reference scan transmitted through free space. (b) Normalized power transmission of the waveguides.

Extraction of the waveguide power loss factor was implemented through the same linear-fit process as described in the previous section. Figure 7(a) plots the relative transmission power at 107 GHz, which is the center frequency of the first passband. Except for a slight deviation from a straight line at the 100 mm length, the transmitted power in dB decreases linearly as the waveguide length increases. The slope of 0.056 dB/mm is the measured waveguide power loss factor at this frequency. It is worth mentioning that time spans of the truncated waveforms utilized in Fig. 6 were short enough so that it was guaranteed no multiple reflections were included in the calculations. The truncation, however, did use sufficiently-long waveforms so that majority of the transmitted power is retained in the calculation.

#137560 - $15.00 USD Received 2 Nov 2010; revised 2 Feb 2011; accepted 2 Feb 2011; published 15 Feb 2011

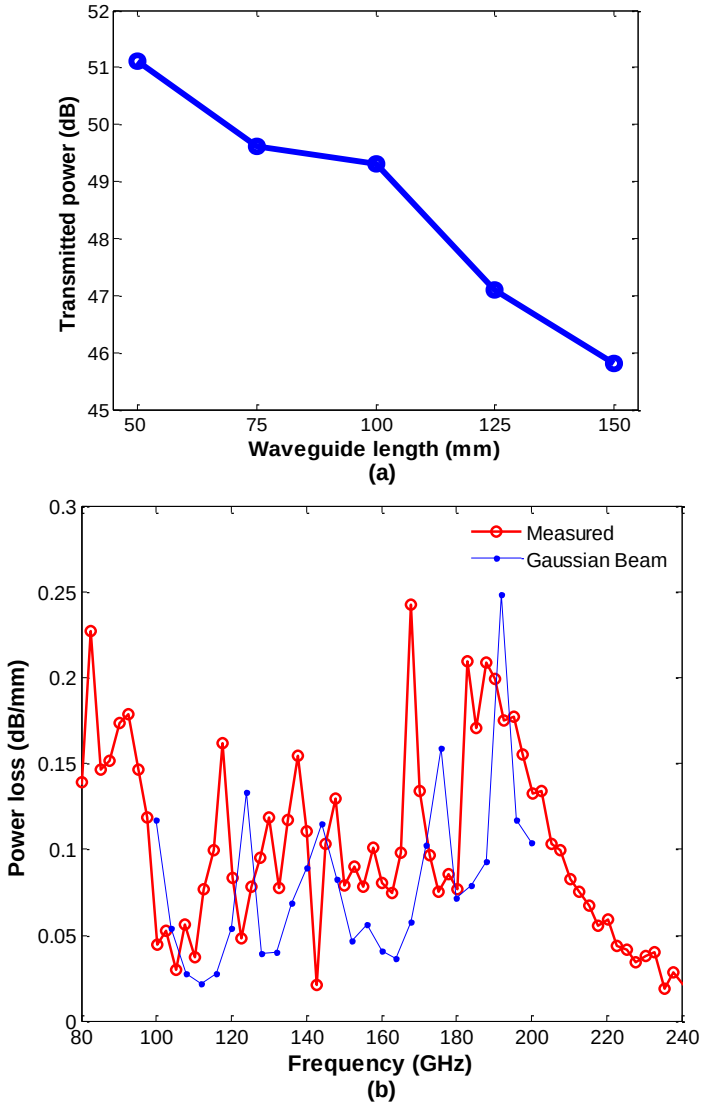

Fig. 7. (a) Semi-log plot of the measured transmitted power in dB versus waveguide length at 107 GHz. Linearly fitted slope gives the power loss factor at this frequency. (b) Measured and simulated waveguide power loss factors under Gaussian beam excitation.

As shown in Fig. 7(b), the measured power loss factors agree quite well with the beam-incidence simulation results. The measured 7-GHz downshift is possibly due to fabrication tolerance, as the air cylinder diameter may not be precisely controlled due to the reduced support material usage in the glossy fabrication mode. Further, the model material has slight dielectric constant dispersion (from 2.8 to 2.73) within the 100-150 GHz range [19], which was not included in the simulations and would also contribute to the discrepancy. Note that the dip at 143 GHz is not reliable because as it is at a deep band-stop frequency (as shown in Fig. 6(b)) for which the signal-to-noise-ratio is not good. Nevertheless, the measurement and the simulation agree well, demonstrating four passbands with low propagation losses at nearby frequencies. The lowest observed power loss factor was 0.03 dB/mm at 105.2 GHz, corresponding to a *Q* factor of 319 at this frequency. As a reference, a standard W-band rectangular waveguide (WR-10, 75-110 GHz) made of copper has a theoretical power attenuation factor of 0.0023-0.0035 dB/mm. However, the practically measured W-band

#137560 - $15.00 USD Received 2 Nov 2010; revised 2 Feb 2011; accepted 2 Feb 2011; published 15 Feb 2011

rectangular waveguide loss reaches 0.01-0.015 dB/mm in [16] and even 0.05-0.07 dB/mm in [17], which are 5 ~ 20 times of the theoretical value. Other reported THz micro-structured waveguides working at similar frequency regime include the sub-wavelength porous fiber by Dupuis *et al.* in [10], hollow-core photonic crystal fiber by Nielson *et al.* in [13], solid-core PCF by Goto *et al.* in [12], etc. The porous fiber demonstrated a very low power loss factor of 0.004 dB/mm at 300 GHz, whereas the solid-core PCF reported a ~0.05 dB/mm loss factor mainly due to material loss. THz micro-porous guidance was claimed to be observed at 200 GHz in [13], however the loss value was not reported. While certainly not presenting the lowest loss coefficient for waveguides at 100 – 300 GHz range, the waveguide reported in this work finds its own advantage in the ease and flexibility of the fabrication process. Moreover, with optimized polymer materials, lower loss should be achieved.

5. Conclusion

A THz waveguide based on a hollow-core electromagnetic crystal structure was designed and then fabricated by polymer jetting rapid prototyping. Quasi-optical THz lenses were also fabricated by the same technique in help with mode-matching the waveguide to free-space Gaussian beams. Results of the power loss factor characterization showed good agreement with simulation. A low transmission loss waveguide operating near 105 GHz was demonstrated with minimal fabrication complexity and cost. Scaling the waveguide to a few hundreds of GHz is feasible under the scope of this fabrication method, and is currently pursued in our lab. Because of the systematic fabrication manor of the rapid prototyping technique, this waveguide can be readily integrated with other THz components such as electromagnetic crystal based horn antennas, THz planar circuits (so that semiconductor based THz source and detector can be readily integrated), and other quasi-optical parts fabricated by the same approach. We anticipate that this will ultimately lead to integrated fully-functional THz systems.

Acknowledgments

This work was supported in part by the National Science Foundation under Awards 0823864 and 0925220, and the state of Arizona under TRIF.

#137560 - $15.00 USD Received 2 Nov 2010; revised 2 Feb 2011; accepted 2 Feb 2011; published 15 Feb 2011